Available online at www.sciencedirect.com
SCIENCE DIRECT
Neuroscience Research 52 (2005) 211–219
Neuroscience Research
www.elsevier.com/locate/neures

Voxel based comparison of glucose metabolism in the differential diagnosis of the multiple system atrophy using statistical parametric mapping

Rahyeong Juh [a], Chi-Un Pae [b], Chang-Uk Lee [b,*], Dongwon Yang [c], Yongan Chung [d], Taesuk Suh [a,*], Boyoung Choe [a]

[a] *Department of Biomedical Engineering, St. Mary' Hospital, The Catholic University of Korea College of Medicine, 505 Banpo-Dong, Seocho-Gu, Seoul 137-701, South Korea*
[b] *Department of Psychiatry, St. Mary' Hospital, The Catholic University of Korea College of Medicine, 505 Banpo-Dong, Seocho-Gu, Seoul 137-701, South Korea*
[c] *Department of Neurology, The Catholic University of Korea College of Medicine, 505 Banpo-Dong, Seocho-Gu, Seoul 137-701, South Korea*
[d] *Department of Nuclear Medicine, The Catholic University of Korea College of Medicine, 505 Banpo-Dong, Seocho-Gu, Seoul 137-701, South Korea*

Received 8 November 2004; accepted 15 March 2005
Available online 26 April 2005

Abstract

Objective: A differential diagnosis of idiopathic parkinsonian disease (IPD) and multiple system atrophy (MSA) is difficult due to their common signs and symptoms. The aim of this ^{18}F-2-fluoro-2 deoxyglucose (^{18}F-FDG) positron emission tomography (PET) study was to compare the regional cerebral glucose metabolism in MSA with that in IPD by statistical parametric mapping (SPM) and image registration.
Methods: The ^{18}F-FDG PET images of MSA and IPD patients were assessed by SPM and image registration to determine metabolic patterns that may be useful in differentiating between the two groups. Eleven patients with MSA, eight patients with IPD and 22 healthy controls participated in the study.
Results: The IPD patients were found to have a significant glucose hypometabolism in comparison with the healthy controls in the prefrontal, lateral frontal, and parietotemporal cortices, and the cingulate and caudate areas ($p \leq 0.01$, 100 voxel-level). In patients with MSA, hypometabolism was observed in the putamen, pons, and cerebellum in comparison with the healthy controls and IPD patients.
Conclusion: The voxel-based analysis of ^{18}F-FDG PET images showed detailed differences between IPD and MSA, which may be useful in differentiating the two disease entities, as evidenced by the correlation of glucose metabolism with disease severity and dopamine agonist medication. The mapping analysis of ^{18}F-FDG PET images might be a useful adjunctive method of a differential diagnosis for parkinsonism in a clinical setting.

Keywords: ^{18}F-FDG PET; Parkinsonism; Statistical parametric mapping

1. Introduction

Parkinsonism is characterized clinically by deficits in the motor function such as tremor, rigidity, bradykinesia, hypokinesia and postural abnormalities. A differential diagnosis between IPD and MSA is usually difficult. MSA is a sporadic adult-onset neurodegenerative disease, which usually presents clinically as a combination of parkinsonism, cerebellar ataxia and autonomic failure. The predominant pathological correlates, namely, olivopontocerebellar atrophy (OPCA) and striatonigral degeneration (SND), of two forms of clinical presentation, are now called the MSA cerebellar type (MSA-C) and MSA parkinsonism (MSA-P) (Poewe and Wenning, 2002). In MSA-C, which is

* Corresponding authors. Tel.: +2 590 2789; fax: +2 536 8744.
E-mail addresses: knpsy@catholic.ac.kr (C.-U. Lee), suhsanta@catholic.ac.kr (T. Suh).

0168-0102/$ – see front matter
doi:10.1016/j.neures.2005.03.010

characterized clinically by predominant cerebellar ataxia, the pathological findings are primarily those of neuronal cell loss and gliosis in the inferior olivary nucleus, pontine nuclei, cerebellar hemispheres and vermis, whereas SND, which has a mainly parkinsonian clinical phenotype, is associated with neuronal cell loss and gliosis in the substantia nigra, putamen, caudate nucleus and globus pallidus. Most cases of OPCA and SND are also accompanied by neurodegeneration in the autonomic nervous system which, when presenting clinically with prominent autonomic failure, has been referred to as the Shy–Drager syndrome. One-half of the patients with the akinetic-rigid variant MSA show a good response to L-dopa, which makes it difficult to distinguish MSA from IPD on the basis of the clinical criteria alone (Brooks, 2000; Thobois et al., 2001). In addition, an early diagnosis of parkinsonism is important not only because of its prognostic implications, but also because of the many treatments options (Schrag et al., 1999, 2000). Although a definite diagnosis of these disorders can only be made by a neuropathological examination, there is a need for the development of additional criteria that will aid in a clinical diagnosis. Generally, these disorders are characterized by distinctive sets of features determined by statistical parametric mapping (SPM) (Acton et al., 1999; Hosaka et al., 2002; Friston, 1995; Ashburner and Friston, 2000). Multimodality imaging techniques such as magnetic resonance imaging (MRI), single photon emission computed tomography (SPECT), and PET have been increasingly used to examine the morphological and functional characteristics of IPD and those related disorders in relation with the diagnosis. Metabolic brain imaging by ^{18}F-FDG PET has become a major tool for investigating age-related brain pathologies (Thobois et al., 2001; Hosaka et al., 2002; Eidelberg et al., 1995). The aim of this study was to describe the voxel-based glucose metabolism in IPD and MSA patients in comparison with that in healthy volunteers.

2. Materials and methods

2.1. Subjects

Eight clinically probable IPD patients (3/5:M/F; age, 67.9 ± 10.7 years) and 11 probable MSA patients (4/7:M/F; age, 58.5 ± 8.4 years) were included in the study. Twenty-two age-matched healthy controls (9/13:M/F, age, 67.8 ± 14.4 years) were examined and used as the controls for the comparison with IPD patients. They had no history of any disease of the central nervous system, and their neurological examination results were normal. All the patients and normal control subjects underwent ^{18}F-FDG PET. The clinical diagnosis of IPD and MSA were accepted on the basis of the Brain Bank criteria and the Quinn criteria, respectively (Hughes et al., 1992; Wenning et al., 1994). The complete clinical data and follow-up information were available at the time of PET, and the diagnosis was made prior to and independent of PET results. The clinical status was also assessed using the unified Parkinson's disease rating scale (UPDRS). All the MSA patients had the non-L-dopa responsive akinetic-rigid syndrome and presented with progressive limb rigidity and bradykinesia associated with an early impairment of balance and gait. Eight patients with IPD had L-dopa responsive akinetic-rigid syndrome without any evidence of cerebellar ataxia, pyramidal and autonomic signs. The patients were aged more than 50 years and their disease was at the Hoehn and Yahr (H&Y) stages II–IV when assessed in the 'off' state. The mean durations of their H&Y stages were 2.3 ± 1.1 years and 2.4 ± 0.8 years for IPD and MSA, respectively. On the basis of UPDRS subscores and follow-up data, severity indexes ranging from 1 to 4 were assigned (1 = absent, 2 = light, 3 = moderate, 4 = severe) to the following symptoms: tremor, akinesia, cerebellar ataxia, cerebellar atrophy, autonomic failure, and gait disturbance (Table 1).

Table 1
Clinical data of IPD, MSA and control groups

Clinical diagnosis	Control (n = 22)	IPD (n = 8)	MSA (n = 11)
Age (years)	67.8 ± 14.4	67.9 ± 10.7	58.5 ± 8.4
Sex (M/F)	9/13	3/5	4/7
Disease duration (month)	–	35.3 ± 26.3	29.3 ± 12.9
H&Y stage (years)	–	2.3 ± 1.1	2.4 ± 0.8
UPDRS		34.8 ± 16.6	41.0 ± 15.9
Semiquantitative symptom score: severity indexes ranging from 1 to 4 was assigned (1 = absent, 2 = light, 3 = moderate, 4 = severe)			
Tremor	–	2.3 ± 1.8	1.8 ± 0.8
Akinesia	–	2.5 ± 0.9	2.3 ± 0.7
Cerebellar ataxia	–	–	2.4 ± 0.9
Cerebellar atrophy	–	–	2.4 ± 0.9

IPD, idiopathic Parkinson's disease; MSA, multiple system atrophy; H&Y, Hoehn and Yahr score; UPDRS, unified Parkinson's disease rating scale. Data are expressed as mean ± S.D. unless indicated otherwise.

2.2. ^{18}F-FDG PET data acquisition and reconstruction

^{18}F-FDG PET scans was performed using an ECAT HR plus and biograph (Siemens Medical System, Inc., Hoffman Estate, IL). It was performed with the subjects under resting conditions with their eyes closed and ears unplugged, comfortably lying in a darkened and quiet room. Forty minutes after injecting 214.6–444 MBq ^{18}F-FDG, a sequence of three 10 min frames was acquired and later summated into a single frame. The images were reconstructed by ordered subset expectation maximization (OSEM) with 16 subsets and 6 iteration reconstruction algorithms (Shepp filter, cut-off frequency at 0.5 cycles per projection element). The dimensions of the reconstructed PET images were a 128 × 128 image matrix with a pixel size of 1.72 mm × 1.72 mm and an interslice distance of 2.43 mm.

2.3. Data analysis

Data were analyzed for any regionally specific effects by SPM in conjunction with MATLAB version 6.1 (Mathworks

Inc., USA) running on Windows NT. After converting the data from DICOM into Analyze format, the images obtained from each subject were spatially transformed to a generic SPM FDG PET template. SPM involves spatially extended statistical processes that are used to characterize regionally specific effects in imaging data (Friston, 1995). SPM combines the use of a general linear model to generate a statistical map and the theory of Gaussian fields to form statistical inferences regarding the regional effects. The image realignment was resliced and registered using a 0.75 quality factor. The cost function for the registration was used in the normalized mutual information (NMI) method and the trilinear interpolation method for each reslice. The NMI for the registrations in SPM resolved the overlap problem to bring about mutual information (MI). Anatomic standardization was performed by a nonlinear transformation using $7 \times 8 \times 7$ basis functions and 16 nonlinear iterations to the SPM PET template. A resulting voxel size of 2 mm × 2 mm × 2 mm was used. The NMI was smoothed with an isotropic Gaussian kernel with a 12 mm.

2.4. Statistical analysis

Data analysis of 19 consecutive patients was performed for a detailed discrimination by group and individual analyses. The effects of global metabolism were removed by normalizing the count of each voxel to the total count of the brain using proportional scaling. The brain image of each patient was compared with those of healthy volunteers at each pixel, using an unpaired two-sample *t*-test based on two contrasts to detect any regional decrease in metabolism. To detect any regional metabolic pattern by SPM, all the images were performed using the appropriate voxel-by-voxel unvaried statistical tests of group comparisons (two-sample *t*-test) within the three groups (IPD versus normal, MSA versus normal, IPD versus MSA) and each patient versus normal controls using an unpaired two-sample *t*-test based on the two contrasts. These were performed using a proportional scaling technique. Proportional scaling basically scales each image according to a reference count, which is the global brain activity, to a physiologically realistic value of 50 ml/dl/min. At a variable voxel height threshold that had a probability value with or without a correction for multiple comparisons, clusters consisting of a minimum of 100 contiguous voxels were considered significantly different. The results were displayed on the three orthogonal planes of an MRI template. The Talairach brain coordinates were estimated by a nonlinear transformation from the Montreal Neurological Institute (MNI, McGill University, Montreal, Quebec, Canada) space to the Talairach (Talairach Daemon Client. Ver.1.1, Research Imaging Center, University of Texas Health Science Center at San Antonio) space (Friston, 1995).

Table 2
Single case analysis of glucose metabolism in patients with IPD ($n = 8$) and MSA ($n = 11$)

Type	Frontal	Parietal	Temporal	Occipital	Cingulate	Caudate	Putamen	Thalamus	Midbrain	Pons	Cerebellum
IPD ($n = 8$)[a]											
PD1	$Z = 3.36$	–	$Z = 5.22$	–	$Z = 3.42$	–	–	–	–	–	$Z = 4.88$ (inc)
PD2	$Z = 4.13$	–	–	$Z = 3.43$	$Z = 3.88$	$Z = 4.51$	–	$Z = 4.69$	$Z = 3.41$		$Z = 3.36$ (inc)
PD3	$Z = 2.98$	–	–	–	–	–	–	–	–	–	–
PD4		$Z = 4.59$	$Z = 5.17$	$Z = 2.85$	$Z = 2.85$	–	–	–	–	–	$Z = 3.83$ (inc)
PD5	$Z = 4.02$	–	–	–	–	$Z = 3.88$	–	–	–	–	–
PD6	–	–	–	–	–	–	–	–	–	–	$Z = 3.25$ (inc)
PD7	$Z = 3.66$	$Z = 5.38$	$Z = 3.66$	$Z = 3.53$	$Z = 4.57$	$Z = 3.53$	–	–	–	–	$Z = 4.44$ (inc)
PD8	$Z = 2.82$	$Z = 3.74$	$Z = 3.87$	$Z = 2.83$							
Frequency # of the 8 (%)	6 (75)	3 (37)	4 (50)	4 (50)	4 (50)	3 (37)	–	1 (12)	1 (12)	–	5 (63) (inc)
MSA ($n = 11$)											
PD1 (MSA-C)	–	–	–	–	–	–	–	–	–	$Z = 3.08$	$Z = 3.34$
PD2 (MSA-C)	–	–	–	–	–	–	–	–	–	$Z = 4.24$	$Z = 3.43$
PD3 (MSA-C)	–	–	–	–	–	–	–	–	–	$Z = 3.28$	$Z = 3.22$
PD4 (MSA-C)	$Z = 4.14$	–	–	–	–	–	–	–	–	$Z = 2.98$	$Z = 2.99$
PD5 (MSA-C)	$Z = 4.03$	$Z = 4.21$	$Z = 4.10$	–	–	–	–	–	–	$Z = 2.85$	$Z = 2.85$
PD6 (MSA-P)	$Z = 4.11$	–	–	–	–	$Z = 4.27$	–	$Z = 4.26$	$Z = 3.95$	$Z = 3.95$	–
PD7 (MSA-P)	–	–	–	–	–	–	$Z = 3.36$	–	–	–	–
PD8 (MSA-P)	$Z = 4.36$	$Z = 5.16$	$Z = 4.94$	–	–	–	$Z = 4.37$	–	–	–	–
PD9 (MSA-P)	$Z = 3.47$	$Z = 3.62$	$Z = 3.12$	–	–	–	$Z = 4.44$	–	–	–	–
PD10 (MSA-P)	$Z = 4.14$	–	–	–	–	–	$Z = 4.25$	–	–	–	–
PD11 (MSA-P)	$Z = 4.14$	–	–	–	–	–	$Z = 4.25$	–	–	–	–
Frequency # of the 11 (%)	7 (64)	3 (27)	3 (27)	–	–	1 (9)	5 (45)	1 (9)	1 (9)	6 (55)	5 (45)

This table shows the locations and peak *Z*-values of a significant decrease in glucose metabolism in each patient with IPD and that with MSA compared with the normal controls. The table lists the most significant *Z*-scores within each cluster ($p \leq 0.01$, 100 voxel-level).

[a] Extent threshold of $p \leq 0.01$, 100 voxel-level. *Z*-value: decreased voxel *Z*-value of the single patient, *Z*-value (inc): voxel *Z*-value of the increased region than normal group.

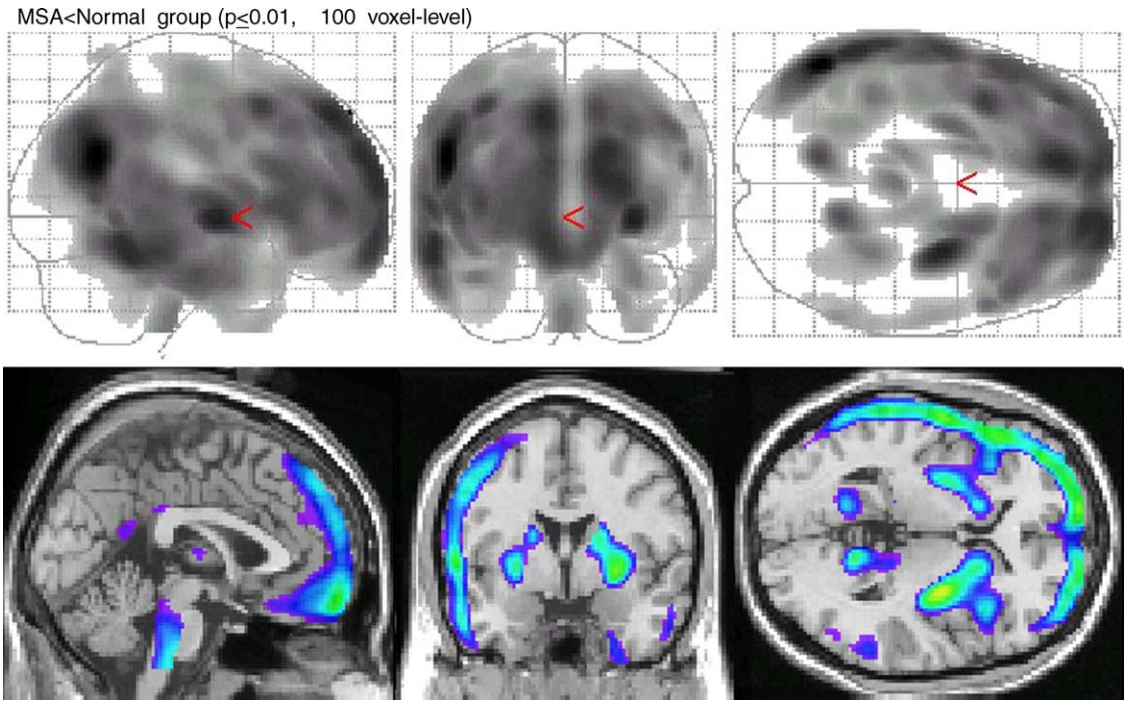

Fig. 1. MSA group vs. normal control group. The SPM glass brain maps of difference in ^{18}F-FDG uptake between MSA patients vs. the normal controls show the contrast of a decreased glucose metabolism in patients. The SPM result shows spatial distribution of regions ($p \leq 0.01, Z > 2.85$) with a significant decrease in glucose metabolism in the MSA group. Images are shown as integrated projections along the sagittal, coronal, and transverse views superimposed on a normalized template MRI. A comparison between the MSA and normal control groups revealed a lower metabolism in the putamen, pons, and cerebellum of the more affected hemisphere in the MSA group.

3. Results

3.1. MSA group versus normal controls

In the MSA group, a significant glucose hypometabolism in the left parietotemporal cortex, frontal cortex, pons, cerebellum, and putamen of the brain was detected as compared with the age-matched normal controls by statistical voxel-based analysis ($p \leq 0.01$, 100 voxel-level) (Table 2, Fig. 1). Table 2 shows the comparison of the most significant *Z*-values in the ^{18}F-FDG PET of each of the single MSA-C and MSA-P patients with those of the normal controls. Fig. 2 shows the results of the SPM of the same slice and same threshold hypometabolism contrast pattern between each of the MSA-C and MSA-P patients and the normal controls. In the analysis of each MSA-C patient, glucose metabolism was significantly decreased in the pons and cerebellum compared with the age-matched normal controls. In addition, the pons *Z*-values ranged from 2.85 to 4.24 and the cerebellum *Z*-values ranged from 2.85 to 3.43. A comparison of each MSA-P patient with the normal controls revealed a statistically significant decrease in metabolism in the left parietotemporal cortex, frontal cortex, and putamen of the brain. The individual analysis, which compared each MSA-P patient with the normal controls, showed that hypometabolism specifically in the putamen, which was not detected in the IPD group, was distributed from a *Z*-score of 3.36 to that of 4.44 (Table 2).

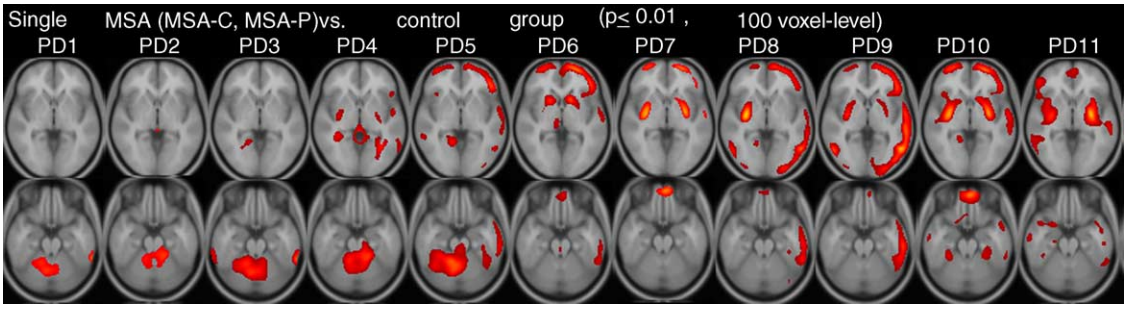

Fig. 2. Single MSA patient vs. normal control group. This image shows the SPM result for each MSA patient compared with normal controls, which shows the same slice and threshold ($p \leq 0.01$, 100 voxel-level). The SPM result shows the spatial distribution of regions with a significant decrease in glucose metabolism in the pons and cerebellum of MSA-C patients and in the putamen of MSA-P patients.

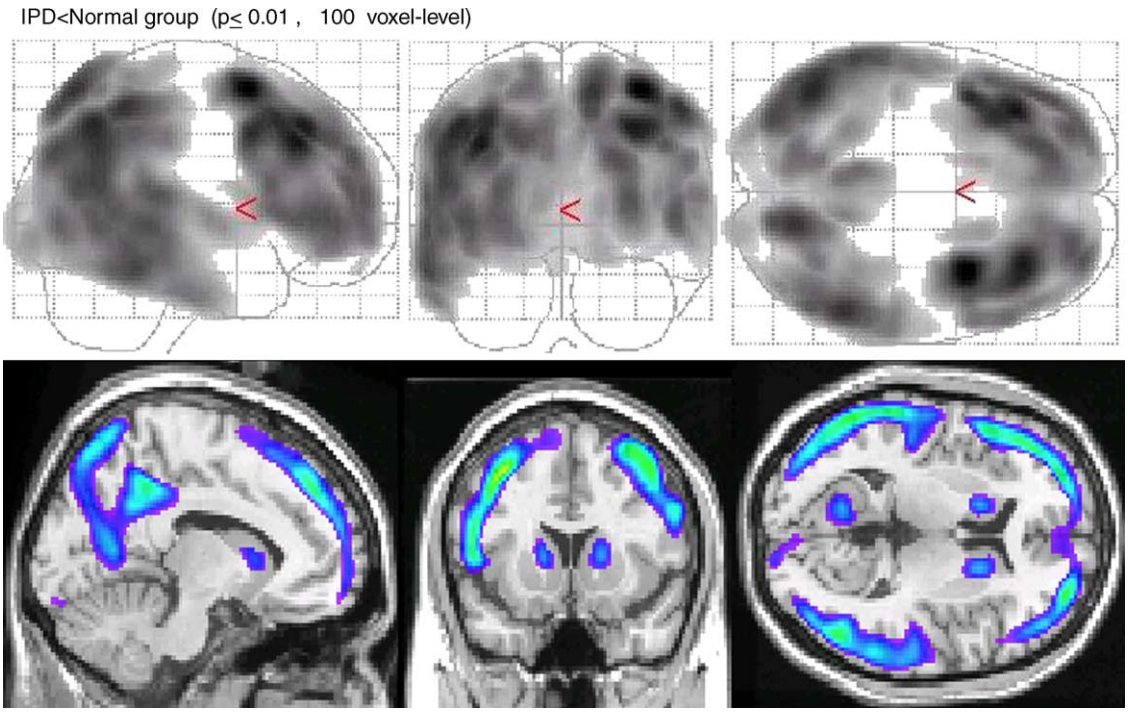

Fig. 3. IPD group vs. normal control group. Specific voxels show a significantly lower glucose metabolism in the IPD group than in the age-matched control group at the threshold of $p \leq 0.01$. Specific voxels in the caudate shows a significantly lower glucose metabolism in the IPD group than in the normal control group.

3.2. IPD patients versus normal controls

The discrimination between the IPD group and the age-matched normal controls was carried out using the extent threshold 100 voxel-level with $p \leq 0.01$. Fig. 3 shows the group differences and Fig. 4 shows the difference between each patient with IPD and the controls at the same slice and threshold. A significant hypometabolism in IPD patients was observed compared with the normal controls in a symmetric subcortical circuit ranging from the caudate to the cingulate. There was also involvement of the prefrontal and lateral frontal cortices, as well as the middle temporal gyrus, right and left bilateral parietal association cortices, and bilateral occipital cortices (Table 2). The contrast, the relative hypermetabolism for IPD patients versus the normal controls revealed significant clusters in the vermis and the cerebellum (Table 3).

3.3. IPD group versus MSA group

A voxel-based comparison by SPM between the eight IPD patients and 11 MSA patients, as shown in Fig. 3, showed hypometabolism in the pons (Z-score = 3.27), cerebellar vermis (Z-score = 2.65), and putamen (Z-score = 3.47) in the

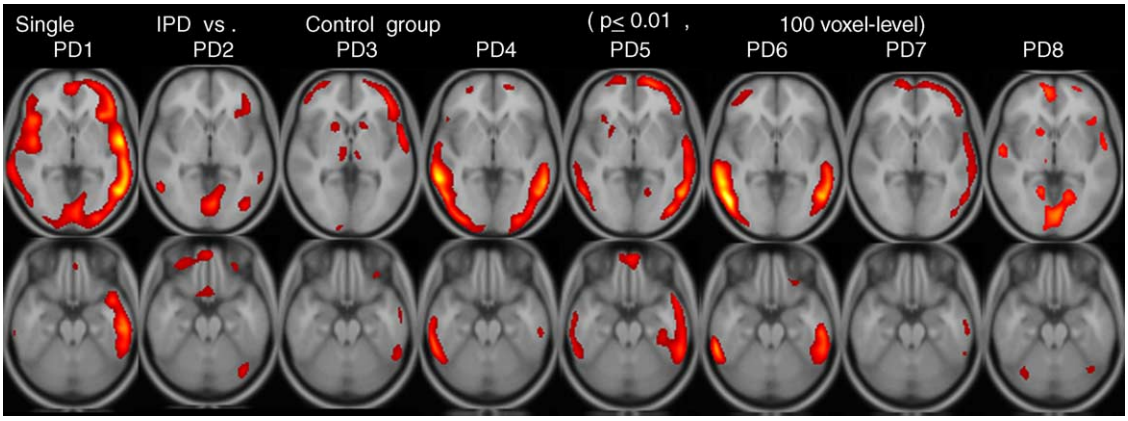

Fig. 4. Single IPD patient vs. normal control group. This image shows the SPM result for each IPD patient compared with normal controls, which shows the same slice and threshold ($p \leq 0.01$, 100 voxel-level).

Table 3
SPM results for group comparison with two-sample *t*-test: IPD patients vs. normal subjects, MSA patients vs. normal subjects, IPD patients vs. MSA patients

Cluster level			Voxel level					Coordinates (mm)			Region
p (cor)	k_E	*p* (uncor)	*p* (FWE-cor)	*p* (FDR-cor)	*T*	Equiv, *Z*	*p* (unc)	*X*	*Y*	*Z*	
IPD < normal											
0.000	10583	0.000	0.000	0.000	8.05	5.74	0.000	36	7	55	Right cerebrum, frontal lobe, middle frontal gyrus
0.000	10562	0.000	0.003	0.000	6.85	5.21	0.000	−36	29	32	Left cerebrum, parietal lobe, inferior parietal lobule
			0.015	0.000	6.16	4.86	0.000	52	−64	22	Right cerebrum, temporal lobe, middle temporal gyrus
			0.023	0.000	5.97	4.76	0.000	60	−44	−22	Right cerebrum, inferior parietal lobule (BA40)
0.000	5825	0.000	0.062	0.000	5.50	4.49	0.000	−52	−64	4	Left cerebrum, middle temporal gyrus (BA 37)
0.640	104	0.182	0.823	0.003	3.95	3.49	0.000	−14	10	7	Left cerebrum, sub-lobar, extra-nuclear, caudate
MSA < normal											
0.000	50654	0.000	0.014	0.005	6.15	4.88	0.000	52	−62	26	Right cerebrum, middle temporal gyrus (BA 39)
0.000	10531	0.000	0.071	0.005	5.43	4.75	0.000	30	37	37	Right cerebrum, frontal lobe, middle frontal gyrus
0.670	2670	0.002	0.026	0.005	5.88	4.74	0.000	−32	−10	−2	Left cerebrum, sub-lobar, lentiform nucleus, putamen
0.009	1010	0.002	0.746	0.009	4.08	3.60	0.000	22	−11	19	Right cerebrum, sub-lobar, extra-nuclear
0.998	635	0.154	0.954	0.013	3.67	3.30	0.000	0	−29	−37	left brainstem, pons
			1.000	0.096	2.23	2.13	0.017	−18	−27	14	Left cerebrum, sub-lobar, thalamus, pulvinar
MSA < IPD											
0.059	1710	0.003	0.885	0.241	4.40	3.47	0.000	34	−21	−1	Right cerebrum, sub-lobar, lentiform nucleus, putamen
0.000	5787	0.000	0.972	0.241	4.03	3.27	0.001	4	−38	−32	Brainstem, pons
0.997	172	0.285	1.000	0.241	3.42	2.89	0.002	−38	−51	−11	Left cerebrum, temporal lobe, fusiform gyrus
0.999	138	0.339	1.000	0.241	3.07	2.66	0.004	−12	−79	−35	Left cerebrum, cerebellum

$p < 0.01$, corrected for multiple comparison with cluster extent threshold $k_E = 100$. cor = corrected; uncor = uncorrected.

MSA patients. However, in the occipital lobe with an extent threshold of 100 voxels and *p*-value of 0.01, a pattern of decreasing metabolism with a *Z*-score of 3.54 was observed in the IPD group compared with the MSA group. This voxel-based comparison by SPM showed that glucose metabolism in the pons, cerebellum and putamen could be used as the variable factor for differentiating between the IPD and MSA groups (Table 2).

4. Discussion

The results of this study showed that SPM could be successfully utilized to analyze the data of ^{18}F-FDG PET. In this study, we observed decreased glucose metabolism in the IPD and MSA patients compared to the normal controls and analyzed the individual single subject and group by statistical pattern analysis and image registration. A comparison of the MSA patients with the normal controls revealed a significant decrease of the glucose metabolism in the parietotemporal (27%) cortex, frontal cortex (64%), pons (55%), cerebellum (45%) and putamen (45%) (Fig. 1, Table 2). The IPD patients were found to show a significant decrease of the glucose metabolism in the parietal cortices (37%), temporal cortices (50%), both frontal cortices (75%), cingulate (50%), occipital (50%) and caudate (37%) (Fig. 3, Table 2). In the eight IPD patients, the *Z*-score indicated that 63% of patients showed an extensive increase in the glucose metabolism in the cerebellum and vermis compared to the normal controls. The pons, cerebellum and putamen may be considered as discriminating factors between patients with IPD and MSA (Fig. 5).

Several studies have revealed that PET can be a useful tool for diagnosing parkinsonism, and reported that the caudate and putamen glucose metabolisms in the MSA patients were lower than those in the normal control, and can also aid in differentiating the MSA from IPD (De Volder et al., 1989; Eidelberg et al., 1995; Schocke et al., 2002). As for SND, in particular the nigrostriatal degeneration type, putaminal atrophy and marginal hyperintensity may be useful for differentiating this disorder from IPD (Schrag et al., 2000; Counsell and Hughes, 1999; Bosman et al., 2003; Taniwaki et al., 2002). The putaminal glucose metabolism of the SND was significantly lower than those

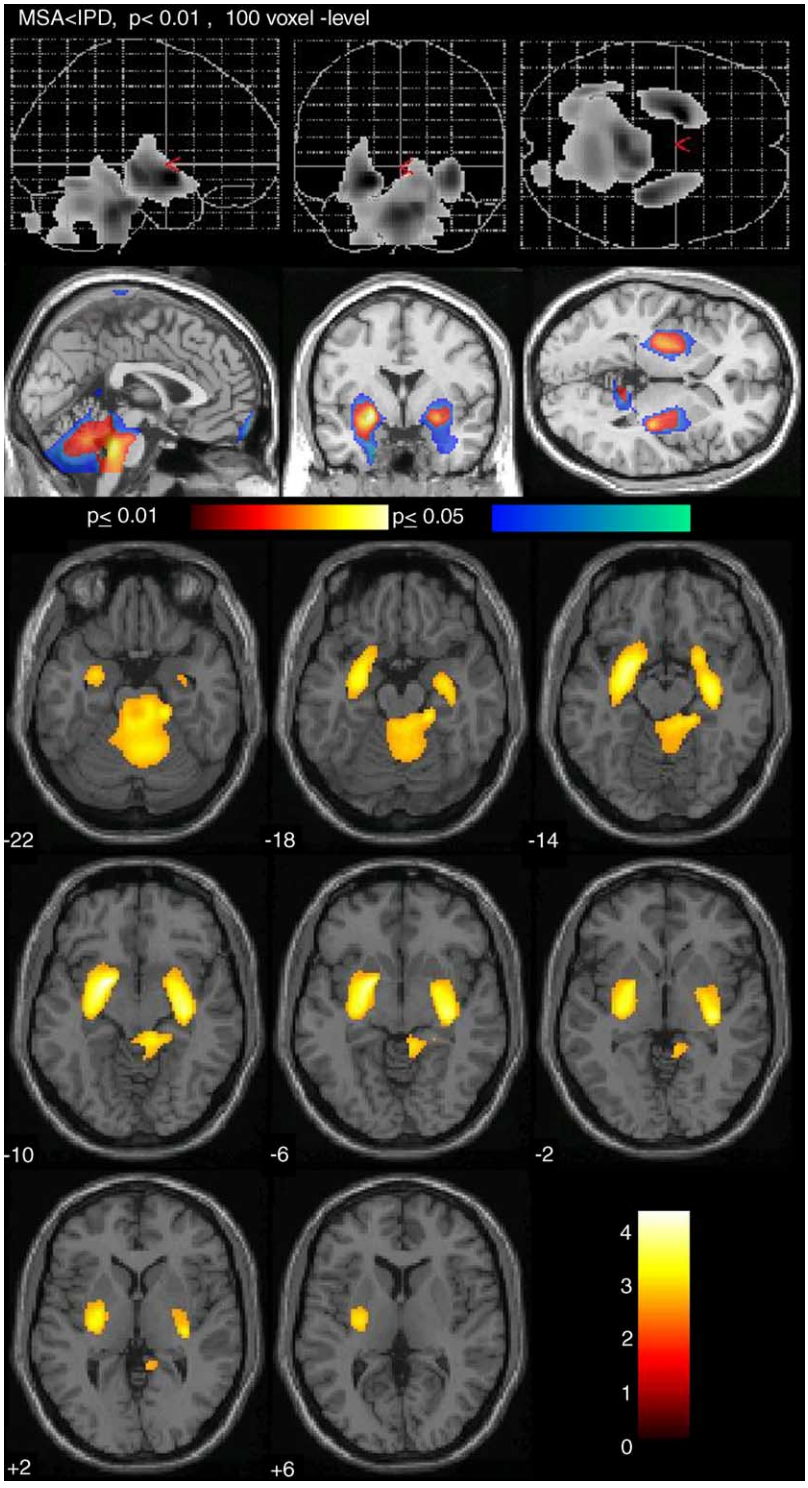

Fig. 5. MSA group vs. IPD group. Discriminating variable factor; hypometabolism in the cerebellum, pons, and putamen in the MSA group compared with that of the IPD group.

of the normal controls and IPD patients. This diminished striatal metabolism is believed to be a distinctive sign compared with the normal controls or IPD patients (Acton et al., 1999; Counsell and Hughes, 1999; Bosman et al., 2003). Significant hypometabolism in the putamen was also observed in our study, which is similar to the previous studies. Moreover, the usefulness of the ^{18}F-FDG for differentiating MSA from IPD has a greater advantage than that of other tracers such as ^{18}F-fluorodopa (FDOPA), ^{11}C-raclopride and ^{123}I-iodobenzamide (IBZM). Several studies have shown that PET studies of the presynaptic nigrostriatal dopamine system using FDOPA provide a relatively poor

discrimination between IPD and MSA because the nigrostriatal dopaminergic neurons degenerate in these disorders (Kim et al., 2002). Brain metabolism studies using FDOPA can only separate healthy subjects from parkinsonism patients, but it is inadequate for discriminating between MSA and IPD because the nigrostriatal dopaminergic neurons degenerate in these disorders (Burn et al., 1994; Ito et al., 1999). Moreover, PET studies using ^{11}C-raclopride have demonstrated decreased postsynaptic striatal D2 receptor binding in MSA patients. Dopamine D2 receptor-binding studies using ^{11}C-raclopride and ^{123}I-IBZM could aid significantly in discriminating the two disorders. The ^{123}I-IBZM uptake is usually lower in the striatal D2 dopamine receptor binding in MSA patients, but the IPD patients in the early stage showed an increase. In addition, Thobois et al. (2001) reported that the ^{11}C-raclopride uptake were lower in the putamen of MSA patients. Although ^{11}C-raclopride shows a very high discrimination capacity, but it is available only in PET centers with an in-house cyclotron.

The MR images of the IPD patients in our present study were grossly normal, apart from subtle mesencephalic changes in an uncertain diagnostic value and this MRI finding result agreed with previous findings consistent with the underlying pathology observed (Schrag et al., 2000; Asato et al., 2000; Schwarz et al., 1999; Yekhlef et al., 2003). On the other hand, some MRI findings indicating MSA represent approximately 10% of degenerative parkinsonian syndromes; therefore, the accompanying atrophy of the lower brainstem, pons, middle cerebellar peduncles and vermis, as well as the pontine cruciform hyperintensity on T2-weighted images also appear to be relevant in the differential diagnosis of MSA (Hosaka et al., 2002; Burn et al., 1994). In our present study, most of the MSA patients also showed a multifocal punctate high signal intensity on T2-weighted images. These problems of morphological distortion and brain atrophy are a limitation in differential comparison between sets of brain images of the patients and normal controls in this study. Therefore, we have attempted to solve these problems, that is, the morphological distortion and brain atrophy through anatomic standardization and image registration using SPM. Indeed, SPM was first developed for use in activation studies of normal subjects, but image realignment and registration for anatomic standardization, spatially normalized into a standard space, and smoothing could be available for application in SPM (Ashburner and Friston, 2000, 1999; Ashburner et al., 1998; Friston, 1995; Wright et al., 1995). SPM involves spatially extended statistical processes that are used to characterize regionally specific effects in imaging data.

Most neurotransmitter imaging data have often been analyzed identifying by drawing the region of interest (ROI) on brain images. Parkinsonism also showed a reduction in the dopaminergic metabolism, confirming reports of some studies using ROI analysis (Fumihiko et al., 2002; Radau et al., 2000). However, identifying is a time-consuming process, prone to bias and could easily miss small areas and overlook areas outside of the ROI. However, anatomical standardization using image registration and voxel-based analysis by SPM that transforms the stereotactic space or spatial normalization is used to overcome the limitation in general ROI analysis (Ashburner and Friston, 2000, 1999; Ashburner et al., 1998; Friston, 1995; Wright et al., 1995). Above all, an anatomical standardization or spatial normalization can be carried out on a set of normal control subjects using the volumes of interest (VOIs) as well as on a voxel-by-voxel basis. Applying statistical analysis to patients suspected of having parkinsonism should also make the diagnosis more sensitive and specific. It should also be possible to use SPM in determining the regional striatal and extrastriatal differences in dopaminergic metabolism. There are other advantages in applying SPM to reduce the sources of error in conventional ROI analyses include the variances in head positioning and ROI placement. Voxel-based analysis using anatomically normalized images minimizes the error arising from ROI positioning. SPM offers a collection of noninteractive techniques that require a spatial fitting of brain images into the standard stereotactic space to facilitate the anatomical accuracy of the subsequent voxel-based analyses. Most of the significant metabolic differences found between the MSA and IPD patients in our present study are consistent with the peculiarity of the ^{18}F-FDG PET pattern.

A limitation of this study was the insufficient numbers of patients and control subjects as a consequence of the limited PET availability. A pathological correlation and a post-mortem evaluation were lacking in our study. Moreover, we could not form a correlation between voxel-based SPM analysis and ROI-based approaches and quantitatively proof superior to voxel-based SPM analysis. Because parkinsonism involves a different pathophysiology in the cortical and subcortical brain structures, a regional assessment of cerebral glucose metabolism might be useful in the differential diagnosis of parkinsonism. In this study, we evaluated the feasibility of this technique in the differential diagnosis of MSA and IPD by SPM using image registration. Although there were some limitations, the statistical difference in glucose meabolism using the noninteractive voxel-based technique can be used a basis to differentiate between MSA from IPD.

In conclusion, in this study, we evaluated the feasibility of using an SPM technique in the differential diagnosis of parkinsonism. The MSA group showed a significant glucose hypometabolism in the cerebellum, pons and putamen compared with the healthy controls, whereas the IPD group showed a significant glucose hypometabolism in the prefrontal, lateral frontal, and parietotemporal cortices, and the cingulate and caudate areas. These findings suggest that measuring glucose metabolism by ^{18}F-FDG PET followed by voxel-based SPM analysis and image registration could be useful in discriminating parkinsonism and in establishing a differential diagnosis.

Acknowledgments

This study was supported by the Korea Institute of Science and Technology Evaluation and Planning (KISTEP) and the Ministry of Science and Technology (MOST) of Korean government.

References

Acton, P.D., Mozley, P.D., Kung, H.F., 1999. Logistic discriminant parametric mapping: a novel method for the pixel-based differential diagnosis of Parkinson's disease. Eur. J. Nucl. Med. 26, 1413–1423.

Asato, R., Akiguchi, I., Masunaga, S., Hashimoto, N., 2000. Magnetic resonance imaging distinguishes progressive supranuclear palsy from multiple system atrophy. J. Neural. Transm. 107, 1427–1436.

Ashburner, J., Friston, K.J., 1999. Nonlinear spatial normalization using basis functions. Hum. Brain Mapping 7 (4), 254–266.

Ashburner, J., Friston, K.J., 2000. Voxel-based morphometry—the methods. Neuroimage 11, 805–821.

Ashburner, J., Hutton, C., Frackowiak, R., Johnsrude, I., Price, C., Friston, K.J., 1998. Identifying global anatomical differences: deformation-based morphometry. Hum. Brain Mapping 6 (5), 348–357.

Bosman, T., Van Laere, K., Santens, P., 2003. Anatomically standardised ^{99m}Tc-ECD brain perfusion SPET allows accurate differentiation between healthy volunteers, multiple system atrophy and idiopathic Parkinson's disease. Eur. J. Nucl. Med. Mol. Imaging 30, 16–24.

Brooks, D.J., 2000. Morphological and functional imaging studies on the diagnosis and progression of Parkinson's disease. J. Neurol. 247 (Suppl. 2:II), 11–18.

Burn, D.J., Sawle, G.V., Brooks, D.J., 1994. Differential diagnosis of Parkinson's disease, multiple system atrophy, and Steele-Richardson-Olszewski syndrome: discriminant analysis of striatal ^{18}F-dopa PET data. J. Neurol. Neurosurg. Psychiatr. 57, 278–284.

Counsell, C., Hughes, A., 1999. Clinical usefulness of MRI in multisystem atrophy. J. Neurol. Neurosurg. Psychiatr. 66, 694.

De Volder, A.G., Francart, J., Laterre, C., Dooms, G., Bol, A., Michel, C., Goffinet, A.M., 1989. Decreased glucose utilization in the striatum and frontal lobe in probable striatonigral degeneration. Ann. Neurol. 26, 239–247.

Eidelberg, D., Moeller, J.R., Ishikawa, T., Dhawan, V., Spetsieris, P., Chaly, T., Belakhlef, A., Mandel, F., Przedborski, S., Fahn, S., 1995. Early differential diagnosis of Parkinson's disease with 18F-fluorodeoxyglucose and positron emission tomography. Neurology 45, 1995–2004.

Friston, K.J., 1995. Commentary and opinion. II. Statistical parametric mapping: ontology and current issues. J. Cereb. Blood Flow Metab. 15, 361–370.

Fumihiko, Y., Akter, H., Tetsuya, S., Tetsuya, I., Yasuhiko, S., Makoto, I., 2002. Template-based method for multiple volumes of interest of human brain PET images. Neuroimage 16, 577–586.

Hosaka, K., Ishii, K., Sakamoto, S., Mori, T., Sasaki, M., Hirono, N., Mori, E., 2002. Voxel-based comparison of regional cerebral glucose metabolism between PSP and corticobasal degeneration. J. Neurol. Sci. 199, 67–71.

Hughes, A.J., Daniel, S.E., Kilford, L., Lees, A.J., 1992. Accuracy of clinical diagnosis of idiopathic Parkinson's disease: a clinico-pathological study of 100 cases. J. Neurol. Neurosurg. Psychiatr. 55, 181–184.

Ito, K., Morrish, P.K., Rakshi, J.S., Uema, T., Ashburner, J., Bailey, D.L., Friston, K.J., Brooks, D.J., 1999. Statistical parametric mapping with ^{18}F-dopa PET shows bilaterally reduced striatal and nigral dopaminergic function in early Parkinson's disease. J. Neurol. Neurosurg. Psychiatr. 66, 754–758.

Kim, Y.J., Ichise, M., Ballinger, J.R., Vines, D., Erami, S.S., Tatschida, T., Lang, A.E., 2002. Combination of dopamine transporter and D2 receptor SPECT in the diagnostic evaluation of PD, MSA, and PSP. Mov. Disord. 17, 303–312.

Poewe, W., Wenning, G., 2002. The differential diagnosis of Parkinson's disease. Eur. J. Neurol. 9 (Suppl. 3), 23–30.

Radau, P.E., Linke, R., Slomka, P.J., Tatsch, K., 2000. Optimization of automated quantification of 123I-IBZM uptake in the striatum applied to parkinsonism. J. Nucl. Med. 41, 220–227.

Schocke, M.F., Seppi, K., Esterhammer, R., Kremser, C., Jaschke, W., Poewe, W., Wenning, G.K., 2002. Diffusion weighted MRI differentiates the Parkinson variant of multiple system atrophy from PD. Neurology 58, 575–580.

Schrag, A., Ben-Shlomo, Y., Quinn, N.P., 1999. Prevalence of progressive supranuclear palsy and multiple system atrophy: a cross-sectional study. Lancet 354, 1771–1775.

Schrag, A., Good, C.D., Miszkiel, K., Morris, H.R., Mathias, C.J., Lees, A.J., Quinn, N.P., 2000. Differentiation of atypical parkinsonian syndromes with routine MRI. Neurology 54, 697–702.

Schwarz, J., Kraft, E., Vogl, T., Arnold, G., Tatsch, K., Oertel, W.H., 1999. Relative quantification of signal on T2-weighted images in the basal ganglia: limited value in differential diagnosis of patients with parkinsonism. Neuroradiology 41, 124–128.

Taniwaki, T., Nakagawa, M., Yamada, T., Yoshida, T., Ohyagi, Y., Sasaki, M., Kuwabara, Y., Tobimatsu, S., Kira, J., 2002. Cerebral metabolic changes in early multiple system atrophy: a PET study. J. Neurol. Sci. 200, 79–84.

Thobois, S., Guillouet, S., Broussolle, E., 2001. Contributions of PET and SPECT to the understanding of the pathophysiology of Parkinson's disease. Neurophysiol. Clin. 31, 321–340.

Wenning, G.K., Ben-Shlomo, Y., Magalhaes, M., Daniel, S.E., Quinn, N.P., 1994. Clinical features and natural history of multiple system atrophy: an analysis of 100 cases. Brain 117, 835–845.

Wright, I.C., McGuire, P.K., Poline, J., Frith, C., Frackowiak, R.S.J., Friston, K.J., 1995. A voxel-based method for the statistical analysis of gray and white matter density applied to schizophrenia. NeuroImage 2, 244–252.

Yekhlef, F., Ballan, G., Macia, F., Delmer, O., Sourgen, C., Tison, F., 2003. Routine MRI for the differential diagnosis of Parkinson's disease, MSA, PSP, and CBD. J. Neural Transm. 110, 151–169.